Chiang Mai J. Sci. 2016; 43(2) : 358-364
http://epg.science.cmu.ac.th/ejournal/
Contributed Paper

Sintered Dual-phase Steels Produced from Pre-alloyed Fe-Cr-Mo Powder

Wananurat Srijampan [a], Monnapas Morakotjinda [b], Rungtip Krataitong [b], Thanyaporn Yotkaew [b], Nattaya Tosangthum [b], Amporn Wiengmoon [a] and Ruangdaj Tongsri *[b]

[a] Department of Physics, Faculty of Science, Naresuan University, Pitsanulok-Nakhon Sawan Road, Tha Pho, Muang, Pitsanulok 65000 Thailand.

[b] Powder Metallurgy Research and Development Unit (PM_RDU), Thailand National Metal and Materials Technology Center, 114 Paholyothin Road, Khlong Nueng, Khlong Luang, PathumThani 12120, Thailand.

*Author for correspondence; e-mail: ruangdt@mtec.or.th

Received: 15 September 2015
Accepted: 26 November 2015

ABSTRACT

The sintered Fe-Cr-Mo-xC steels (where x = 0.05, 0.15, 0.25, 0.35 and 0.45 wt.% C) were produced by vacuum sintering and followed by slow cooling. The sintered steels showed microstructures consisting of mixed $\alpha + \alpha'$ phases. The formation of α' phase was discussed with respect to the classical model for bainitic transformation. The morphologies of the α' phase regions changed from a thick film to a dark island to a bulk form with increasing C content. With the added C contents < 0.25 wt.%, the sintered steels showed low tensile strength and hardness but high ductility. When the C contents ≥ 0.25 wt.%, the sintered Fe-Cr-Mo-xC steels gained strength from the α' phase, whose volume fraction was increased with increasing C content.

Keywords: sintered dual-phase steels, polygonal ferrite, bainite, mechanical property

1. INTRODUCTION

Dual phase (DP) steels are categorized into a grade of steel that its microstructure combines of ferrite (soft matrix phase) and martensite (hard dispersed phase). This microstructure results in a great combination of strength and ductility. Specifically, the microstructure of DP steels is composed of soft ferrite matrix and 10-40% of hard martensite or martensite-austenite (M-A) particles [1]. This type of microstructure allows achieving the ultimate tensile strength (UTS) in the range of 500-1200 MPa. For some applications, also bainitic constituent may be desirable in the DP steel microstructure. The strength of the DP steel microstructure is controlled by the amount of martensite and ductility by the size and distribution of this phase. The UTS of DP steels increased with increasing the volume fraction as well as the tensile strength of martensite. [2].

In the production of wrought DP steels, different materials processing routes can be employed. One example of the process, it

consists of hot rolling at intercritical temperatures, at which the microstructure consists of body-centered cubic (bcc) ferrite or a phase and face-centered cubic (fcc) austenite or g phase with desired volume fraction ratio, quenching to below martensite start (M_S) temperatures and isothermal annealing at such temperatures [1]. The two-step heat treatment comprising of (i) soaking a steel above the transformation temperature A_{C3} followed by air/water quenching and (ii) soaking a steel above the transformation temperature A_{C1} followed by water quenching, can also be employed for producing DP steels [3]. The variant of the heat treatment can be done by air cooling after soaking a steel above the transformation temperature A_{C3} followed by water quenching from temperatures above the transformation temperature A_{C1} to room temperature. The materials processing routes for producing wrought DP steels are thus considered as complicated processes.

In the powder metallurgical route, consisting of pressing and sintering formulated powder compacts, the physical densification will occur simultaneously with the $\alpha \rightarrow \gamma$ transformation and the dissolution of graphite or carbon (C) into the γ matrix. During the cooling after sintering, the transformations of $\gamma \rightarrow \alpha$ or other structures are the keys for manipulating the sintered steel microstructures. According to the continuous cooling transformation diagrams for the sintered Fe-3.0Cr-0.5Mo-*y*C steels (where $y \geq 0.3$ wt.% C) [4], there is possibility that the mixed a + bainite (α') microstructure will develop in some sintered steels. The formation of the α' structure in bulk steels, particularly steel sheets, has been investigated intensively in the literatures [5-13]. However, the powder metallurgical route employed in this study is different from the α' steel sheet forming methods employed in [5-13]. It is worth investigating the α' structure formation in sintered steels.

In addition, the carbide associated with the microstructural development is also worth studying. The iron carbide Fe_3C or cementite is common carbide found in the α' structure. However, there are other carbides including M_7C_3, M_6C and $M_{23}C_6$ observed in as-cast Fe-Cr-Mo-W-C iron [14, 15]. The experimental sintered steels in this work have compositions of Fe-3.0 Cr-0.5Mo-*x*C steels (where x = 0.05, 0.15, 0.25, 0.35 and 0.45 wt.% C). This work aims to find the carbon (C) contents, at which the microstructure of the sintered Fe-3.0 Cr-0.5Mo-C steels consists of mixed $\alpha + \alpha'$ phases. The objective also covers the relationship between microstructure and mechanical properties of the sintered Fe-3.0Cr-0.5Mo-*x*C steels.

2. MATERIALS AND METHODS

The pre-alloyed Fe-3.0Cr-0.5Mo steel powder (Hoganas, Sweden) was admixed with different C contents of 0.05, 0.15, 0.25, 0.35 and 0.45 wt.%. The admixed powders were compacted into tensile test bars with green densities of 6.5 g/cm^3. Sintering of the green specimens was conducted in a vacuum furnace at 1280°C for 45 min. After sintering, the sintered steels were cooled in the furnace with the cooling rate of 0.1°C/s. The sintered specimens were cut, mounted and ground using silicon carbide (SiC) papers. Then the ground specimen surface was polished using a diamond paste. The polished specimen surface was finally etched with Picral acid. Microstructures of the sintered steels were observed using optical microscopy (OM). Tensile property test was conducted using Universal Testing Machine (Instron 8801, S/N) H2059). The test was conducted following the ASTM E8/E8M-15a Standard Test Methods for

Tension Testing of Metallic Materials. Materials hardness was tested using Hardness Tester (Instron-Wolpert930/250). The hardness Rockwell scale F (HRF) was measured. In the test a load of 588.40 N was pressed through an indentor of 1.588 mm steel sphere. The hardness values were obtained following the ASTM E18: Standard methods for Rockwell hardness and Rockwell superficial hardness of metallic materials.

3. RESULTS AND DISCUSSION

3.1 Microstructure

The OM images of the sintered Fe-Cr-Mo-*x*C steels (where x = 0.0, 0.05, 0.15, 0.25, 0.35 and 045 wt.% C) are shown in Figure 1. Without C addition (Figure 1a) the sintered Fe-Cr-Mo steel showed polygonal ferritic (PF) grains and pores within gains, along grain boundaries and at grain corners. With 0.05 wt.% C addition (Fig. 1b), the majority of microstructural features was still dominated by PF grains. Some grain boundary thickening was observed as thick films (arrowed). The addition of 0.15 wt.% C (Figure 1c) resulted information of dark islands (marked as IS) along PF grain boundaries and at PF grain corners. Microhardness of the dark islands was about 369 HV0.01. The increases of the dark island volume fractions with increasing C contents were more obvious in the sintered Fe-Cr-Mo steels with C contents equal or higher than 0.25 2t.% C (Figure 1d-1f). The domination of the dark islands over the PF grains was clearly evidenced in Figure 1f, in which the dark islands nearly occupied the whole microstructure. The structural feature of the dark island was characterized by light dendritic-like ferrites decorated with dark particles along ferrite/ferrite boundaries. No parallel laminar structures of ferrite and cementite (Fe_3C), the characteristic of pearlite, were observed.

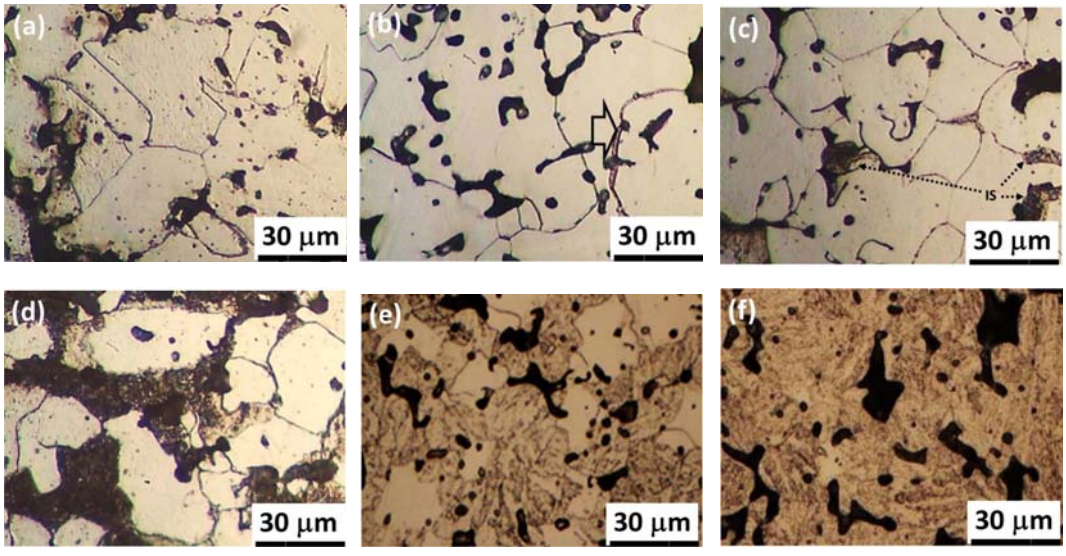

Figure 1. OM images of the sintered Fe-Cr-Mo-xC steels with (a) 0.0, (b) 0.05, (c) 0.15, (d) 0.25, (e) 0.35 and (f) 0.45 wt.% C.

3.2 Microstructural Development

A series of microstructural development given in Figure 1 is interesting due to the absence of pearlite structure, the common microstructural feature of the Fe-C alloy system. The dark phase is gradually developed, from a thick film to an island to a bulk, with its volume fraction increase proportional to the increasing C content in the sintered Fe-Cr-Mo-*x*C steels. Thus the evolution of the dark phase depends strongly on the C distribution and the formation of metal carbide precipitates. Several forms of metal carbides can be formed due to the reaction of C with transition metals, such as Fe, Cr and Mo in cast irons and steels, for example, $M_{23}C_6$, M_6C. M_7C_3 [14, 15]. The thermodynamic study on the Fe-Cr-Mo-C system, using Thermo-Cal software, indicates the theoretical formation possibility of such carbides [4]. However, the carbides of Cr and Mo are not be detected in the sintered Fe-3.0Cr-0.5Mo-*y*C steels (with $y \geq 0.3$ wt.%) due to sluggish diffusion of Cr and Mo in the Fe matrix. Thus only the carbide of Fe or specifically cementite is assumed to form in the sintered Fe-Cr-Mo-*x*C steels.

The microstructural development of the sintered Fe-Cr-Mo-*x*C steels during one sintering cycle (consisting of heating, holding or sintering and cooling), may be depicted by using Figure 2. The microstructural development starts with step (a) of Figure 2, in which the pre-alloyed Fe-Cr-Mo powder with bcc structure of the α phase is mixed and compacted with graphite. No reaction occurs in this step. The maximum solid solubility of C in γ-Fe is ~ 2.0 wt.% C [16], which is much higher than the maximum C content (0.45 wt.%) added to the sintered Fe-Cr-Mo-*x*C steels. Thus during the sintering process in step (b) of Figure 2, all carbon atoms diffuse into the pre-alloyed Fe-Cr-Mo powder matrix, whose structure transforms from α to γ structure during heating the Fe-Cr-Mo-*x*C powder compacts to the sintering temperature and holding at the sintering temperature. The transformation temperature of $\alpha \rightarrow \gamma$ is 912°C for pure Fe [16]. This temperature is reduced with increasing C content, i.e., the temperature of 727°C or the eutectoid temperature is required for the transformation of $\alpha \rightarrow \gamma$ the Fe-0.76 wt.% C steel.

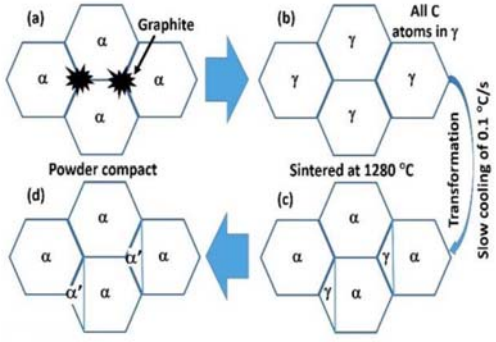

Figure 2. The conceptual sketch of microstructural development in the sintered Fe-Cr-Mo-*x*C steels.

During cooling, the C content exceeding its maximum solid solubility in the a phase will be ejected ahead of the growing front of PF grains (α phase) into the non-transformed γ phase (step (c) of Figure 2). The C ejection is due to the very low solid solubility of C in α-Fe. The very low solubility of carbon in ferrite is reported to be ~0.022 wt. % at about 1000 K (727°C) [17]. Different value of the C solubility in α-Fe is found to be 0.0176 wt.% at the eutectoid temperature of 727°C [18]. The non-transformed γ phase will be supersaturated with C atoms and stable at high temperatures. With further cooling, to the transformation temperature of $\gamma \rightarrow$ bainite (α') or the bainite start (B_s) temperature, the upper bainite (UB) is formed.

The UB formation instead of the pearlite

one is due to the effects of alloying elements on the transformation curves of the Fe-Cr-Mo-*x*C steels. The C, Cr and Mo additions push the transformation nose of the α-phase toward the right-hand side of the diagram as shown in Figure 3 [5, 6]. The Cr and Mo additions also push the transformation nose of the pearlite (α + Fe_3C) toward the right-hand side. However, the transformation nose of the α phase is on the left-hand side farther than that of the pearlite. This means that the Cr and Mo additions will promote the α′ structure formation under slower cooling rates by pushing the pearlite transformation nose to the right-hand side whereas the transformation under the same slow cooling rates cannot avoid the α phase formation. This is the strategy for designing the sintered steels with mixed α+α′ microstructures. The OM microstructures of the sintered Fe-Cr-Mo-*x*C steels with low C contents of up to 0.45 wt.% (Figure 1) confirm the pearlite formation suppression by Cr and Mo additions.

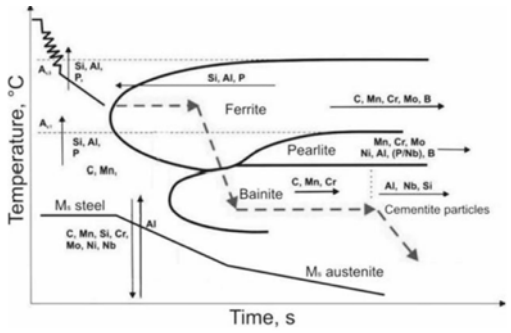

Figure 3. Effects of elements on transformation in steels [5, 6].

The formation of the dark phase is closely related to the UB structure. The UB formation is discussed as follows. The classical model for UB is given in numerous literatures including [7-13].

According to the model (Figure 4) given in [8, 10, 13], the C-supersaturated plates form at high temperatures in the C-supersaturated g regions (marked γ in step (c) of Figure 2). The C atoms diffuse from the C-supersaturated plates to the γ phase in the inter-plate regions. The plates become the α′ phase. The precipitation of the cementite in the γ phase in the inter-plate regions consumes most of dissolved C atoms. The γ phase stability is much reduced due to C depletion and finally it transforms to the α′ phase.

The reason for the bainitic ferrites having dendritic-like shape instead of lenticular shape ferrites is attributed to the longer period of time allowed for C atoms to diffuse from the C-supersaturated plates to the γ phase in the inter-plate regions and the cementite precipitation. It is noticed that when the added C is 0.45 wt.%, the ejection of C atoms ahead of the growing front of the α phase seems to be difficult as the high C concentration is all over the sintered material. It is assumed that the C-supersaturated γ phase is stable until the temperature is reduced to the B_S temperature, at which the C-supersaturated plates are formed all over the microstructure. After that the UB is developed according the mechanism given in Figure 4.

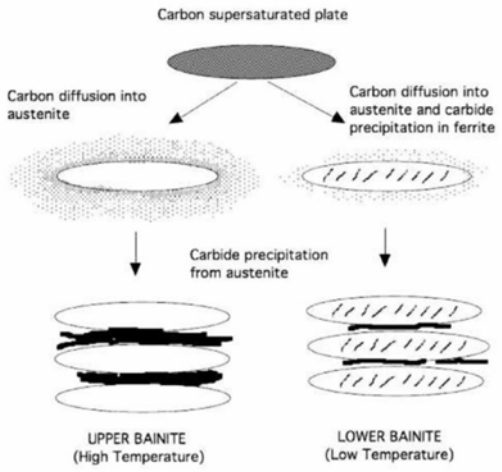

Figure 4. Growth and development of upper or lower bainite after [8, 10, 13].

3.3 Mechanical Property

The UTS and yield strength of the sintered steels increased slightly when the C contents were < 0.25 wt.% (Figure 5). When the C contents ≥ 0.25 wt.%, the sharp increase of tensile strengths could be observed. The increase of the sintered steel hardness with increasing C content showed a similar trend to that of tensile strength. The elongation value was inversely proportional to the C content.

Regardless of the porosity effect, the relationship between the microstructure (Figure 1) and the mechanical property (Figure 5) can be drawn out as follows. With the added C contents < 0.25 wt.%, the majority of the microstructure consists of PF grains, which has low tensile strength and hardness but high ductility. The mechanical property of the sintered Fe-Cr-Mo-*x*C steels (x < 0.25 wt.%) is dominated by the mechanical properties of the PF grains. When the α' phase volume fraction is increased due to the additions of C contents ≥ 0.25 wt.%, the sintered Fe-Cr-Mo-*x*C steels gain strength from the α' phase.

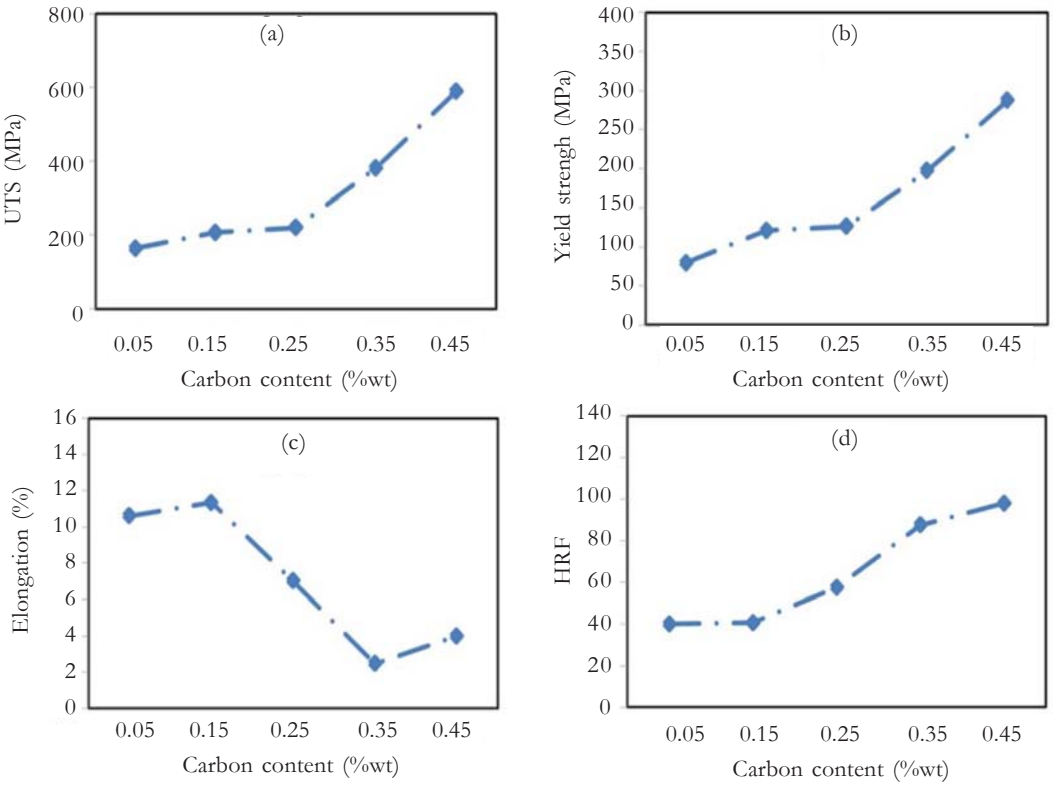

Figure 5. Mechanical properties of the sintered Fe-Cr-Mo-*x*C steels.

4. CONCLUSIONS

The sintered Fe-Cr-Mo-*x*C steels (where x = 0.05, 0.15, 0.25, 0.35 and 0.45 wt.% C), produced by slow cooling after sintering, showed microstructures consisting of mixed $\alpha + \alpha'$ phases. The morphologies of the α' phase changed from a thick film to a dark island to a bulk form with increasing C content. With the added C contents < 0.25 wt.%, the sintered steels showed low tensile strength and hardness but high ductility. When the C contents ≥ 0.25 wt.%,

the sintered Fe-Cr-Mo-*x*C steels gained strength from the α′ phase, whose volume fraction was increased with increasing C content.

5. ACKNOWLEDGEMENT

The first author is financial supported by TGIST scholarship of NSTDA. She is grateful for such kind support. The authors are grateful for financial support from National Metal and Materials Technology Center (MTEC), Pathum Thani, Thailand, under the project MT-B-58-MET-07-269-I. With the courtesy of ACME International (Thailand) Co., Ltd., the prealloyed Fe-Cr-Mo steel powder is available for investigation and the authors are grateful for such in-kind support.

REFERENCES

[1] Kuziak R., Kawalla R., Waengler S., *Arch. Civ. Mech. Eng.*, 2008; **8**: 103-117. DOI 10.1016/S1644-9665(12)60197-6.

[2] Chen H.C. and Cheng G.H., *J. Mater. Sci.*, 1989; **24**: 1991-1994. DOI 10.1007/BF02385411.

[3] Adamczyk J. and Grajcar A., *JAMME.*, 2007; **22**: 13-20.

[4] Yu Y., Thermodynamics and kinetics behaviours of Astaloy CrM; Available at http://www.hoganas.com/Documents/Published%20Articles/2000/Thermodynamic_and_kinetic_behaviours_of_astaloy.pdf.

[5] Lis A.K. and Gajda B., *JAMME.*, 2006; **15**: 127-134.

[6] Grajcar A., Zalecki W. and Kuziak R., *JAMME.*, 2011; **45**: 115-124.

[7] Bhadeshia H.K.D.H. and Edmonds D.V., *Acta Metall.*, 1980; **28**: 1265-1273.

[8] Takahashi M. and Bhadeshia H.K.D.H., *Mater. Sci. Technol.*, 1990; **6**: 592-603.

[9] Fang H.S., Wang J.J. and Zheng Y.K., *Metall. Mater. Trans. A.*, 1994; **25**: 2001-2007.

[10] Bhadeshia H.K.D.H., *J. Phys. IV France.*, 1997; **7**: C5-367-C5-376. DOI 10.1051/jp4:1997558.

[11] Bhadeshia H.K.D.H., *Bainite in steels*, Institute of Materials, London, 2001.

[12] Bhadeshia H.K.D.H., *Proc. R. Soc. A.*, 2010; **466**: 3-18. DOI 10.1098/rspa.2009.0407.

[13] Podder A.S., *Tempering of a Mixture of Bainite and Retained Austenite*, PhD Thesis, University of Cambridge, UK, 2011.

[14] Imurai S., Thanachayanont C., Pearce J.T.H., Tsuda K. and Chairuangsri T., *Mater. Charact.*, 2014; **90**: 99-112. DOI 10.1016/j.matchar.2014.01.014.

[15] Imurai S., Thanachayanont C., Pearce J.T.H., Tsuda K. and Chairuangsri T., *Mater. Charact.*, 2015; **99**: 52-60. DOI 10.1016/j.matchar.2014.11.012

[16] Okamoto H., *J. Phase Equilib,*. 1992; **13**: 543-565.

[17] Jiang D.E. and Carter E.A., *Phys. Rev. B.*, 2003; **67**: 214103. DOI 10.1103/PhysRevB.67.214103

[18] Lobo J.A. and Geiger G.H., *Metall. Trans. A.*, 1976; **7**: 1347-1357.